gear TECHNOLOGY®

JUL 2016

ON CLOSER INSPECTION

- LAB QUALITY ON THE SHOP FLOOR
- AUTOMATED OPTICAL INSPECTION
- CLOSED-LOOP GEAR MANUFACTURING

CHECKING UP ON YOUR HEAT TREATER

IMTS2016 — FIRST LOOK

Hybrid Hertzian and FE-Based Helical Gear-Loaded Tooth Contact Analysis and Comparison with FE

Paul Langlois, Baydu Al and Owen Harris

A loaded tooth contact analysis model for helical gears combining an FE representation of bending and base rotation stiffness of teeth with a Hertzian contact formalism for contact stiffness is presented. Comparison with full 3-D FE contact analysis and the tooth contact analysis program LDP is made. Correlation with the 3-D FE contact analysis is good. For the low-helix angle gear pair under consideration, it is shown that it is important to include the phenomenon of extended contact at the tips of the gear teeth in such hybrid tooth contact models for correlation with the FE analysis at high loads. It is further shown that LDP underestimates the mean transmission error for helical gears when compared to the FE analysis results. A possible cause of this underestimation is presented. A second helical gear example is presented with comparison with results available in the literature.

Introduction

Gear-loaded tooth contact analysis is an important tool for the design and analysis of gear performance within transmission and driveline systems. Methods for the calculation of tooth contact conditions have been discussed in the literature for many years. A number of early review articles include (Refs. 1–3). A number of commercial tools are available that perform such calculations. These specialized tools are used extensively within the industry due to their fast setup and analysis times. While similarities between tools are significant, they differ in implementation and significant differences in results can be found. The most important difference between methods is in the representation of gear tooth and blank stiffness used. Methods using a combination of finite element models to capture the bending and base rotation stiffness and Hertzian formalisms to capture the local contact deflections are considered among the state of the art.

Performing loaded tooth contact analysis in a general FE package requires a very fine mesh in order to accurately capture the Hertzian deflections local to the contact, and therefore are very time consuming to set up and run. As a result, such an approach is rarely used in industry as a design-and-analysis tool. However, it can be considered as a benchmark analysis providing a means of validation of the assumptions made within specialized gear tooth contact analysis models.

In this paper we present a hybrid FE and Hertzian-based loaded tooth contact model — with particular emphasis on the requirements for helical gears — and discuss its relation to other models presented in the literature. We perform an extensive comparison with a loaded tooth contact calculation using a commercial FE package showing good correlation for TE results. Further comparison is made with another well-known specialized loaded tooth contact analysis tool — *LDP* (Ref. 4).

Methodology

Specialized loaded tooth contact analysis model. The following assumptions are made within all calculations in this study:

- The effect of friction is neglected
- The effect of the lubricant is not considered
- Dynamic effects are not considered

A further common assumption is made in the specialized gear tooth contact analysis discussed here:

- Deflections are sufficiently small that the contact points and normals do not move from their theoretical no-load locations

Where the effect of extended tip contact is being considered, potential contact points along the tips of the teeth are included that are not in contact under no-load conditions. This fourth assumption is implicitly not made in the FE analyses presented, where surface-to-surface contact elements are used and the region of contact calculated during the analysis.

The model presented is based on that outlined in (Ref. 5). Inputs include torque, gear macro and microgeometry (flank modifications) and misalignment at the gear mesh. The analysis is quasi-static, performed at a specified number of steps through the mesh cycle. At each step, unloaded potential contact lines are calculated from the gear macro geometries, relative locations and rotations. Potential contact lines are divided into strips (Fig. 1) and contact points expressed in a 2-D coordinate system as distance along face width and roll angle.

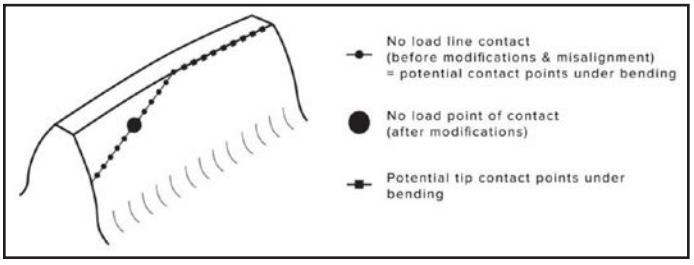

Figure 1 Potential contact line for helical gear tooth with flank modifications and extended contact along gear tip.

Compatibility and force equilibrium conditions relating the discretized contact points are formulated and solved.

At any point, *k*, in the proposed contact zone, the sum of elastic deformations and initial separations must be greater than or equal to the rigid body approach.

$$U_k^1 + U_k^2 + \varepsilon_k - \alpha \geq 0 \quad (1)$$

Where:

1, 2 label the pinion and wheel respectively

U_k^i Is the elastic deformation of gear i at point k
$\mathfrak{E}_k$ Is the initial separation at point k
α Is the rigid body approach

The sum of all the forces acting on the discrete points of contact must balance with the applied load normal to the surface.

$$\Sigma_k F_k = F \tag{2}$$

Where:
F_k Is the normal force at strip k
F Is the total applied normal force due to the applied torque

The formulation of the elastic deformations used in this study is discussed later in this paper. Equations 1 and 2 are solved for F_k, U_k^i, and α, giving the load distribution across the contact lines the elastic deformations at each contact point pair and the rigid body approach.

Helical gear-specific considerations. Some care needs to be taken when formulating the contact problem for helical gears. For spur gears the transverse and normal planes coincide and the components of Equations 1 and 2 are all expressed in the transverse plane normal to the flank profile.

Transmission error is usually expressed as a linear dimension in the transverse line of action

$$TE = r_b^1\theta^1 - r_b^2\theta^2 \tag{3}$$

Where:
r_b^i Is the base radius of gear i
θ^i Is the rotation of gear i

For spur gears the rigid body approach α in Equation 1 is equal to the linear transmission error (TE) in Equation 3.

For helical gears the forces at the contact lie normal to the helix. Care must be taken in which direction the elastic deformations, initial separations and rigid body approach are expressed in and the relationship between the rigid body approach and transmission error. Each component in Equations 1 and 2 can be expressed and solved in a direction normal to the flank and normal to the helix. The rigid body approach, defined in the normal plane, is related to the transmission error, defined in the transverse plane (Fig. 2).

$$\alpha = TE\cos\beta_b \tag{4}$$

Where:
β_b Is the base helix angle

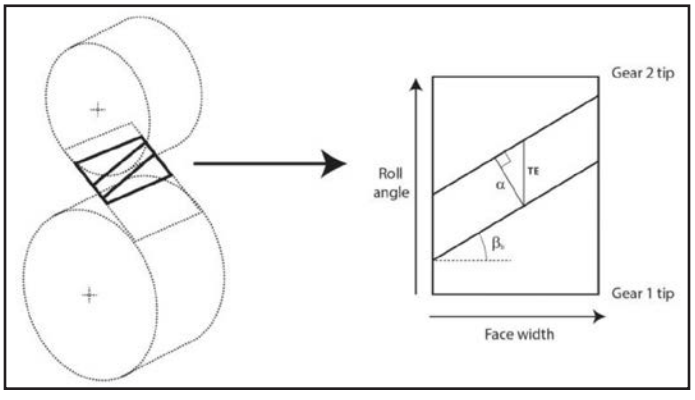

Figure 2 Relationship between TE and normal rigid body approach (α) shown in the plane of action extended off line-of-action contact at gear tips.

Extended off-line-of-action-contact at gear tips. For specialized gear tooth contact models the potential contact points are often limited to the no-load contact points for the corresponding conjugate gears before microgeometry and misalignment are applied (Fig. 1). However, due to the deflections under load (and manufacturing errors), the tips of the teeth may come into contact at points which nominally would not be in contact (those indicated by a square in Fig. 1). Such contact is known in the literature as "off-line of action contact," "corner contact" or "contact outside the normal path of contact." The effect is to increase the operating contact ratio, but also to significantly raise contact stresses due to non-involute contact; this is the main motivation for applying tip relief modifications to gear flanks.

Saeger (Ref. 6) discussed the separation of gear teeth at approach and recess and the possibility of corner contact. Steward (Refs. 7–8) provides a calculation of the off-line-of-action transmission error, together with the corresponding meshing points. Lin et al (Ref. 9) and Singh (Ref. 10) provide equivalent expressions to those of Steward. Munro (Ref. 11) discusses a reformulation of the expressions of Lin et al, together with a number of approximations. The focus of all of these studies is spur gears. Although some mention is given to helical gears, there is little demonstration of the effect of extended tip contact for helical gears on transmission error.

In order to include the effect of extended tip contact in our model, we calculate the potential points of contact in face width and roll angle space and include them in the contact zone points of Equations 1 and 2. The gap between the contacting flanks at these points is calculated according to (Ref. 10) and included in the initial separations of (Eq. 1). The expressions are relatively lengthy and are thus omitted here for brevity.

Hybrid Hertzian and FE-based tooth contact analysis. In the class of models considered here the elastic deformations in Equation 1 are separated into two parts. The bending stiffness and base rotation of the teeth are included via an FE model of the gear. The Hertzian contact stiffness of each strip is considered separately via a Hertzian line contact formalism.

$$U_k^1 + U_k^2 = (C^1F)_k + (C^2F)_k + h_k(F_k) \tag{5}$$

Where:
C^i Is the FE compliance matrix relating the contact points on gear i in the direction normal to the flank
F Is the vector of forces normal to the flank
$h_k(F_k)$ Is the Hertzian deflection normal to the flank at point pair k as a function of the normal load F_k at k

One of the earliest hybrid FE and Hertzian based gear tooth contact models was developed by Vedmar (Ref. 12). Steward (Refs. 7–8) developed such a method for wide face width spur gears, which was subsequently developed further for helical gears. Prabhu (Refs. 13–14) developed a similar method that was the basis of the thin-rimmed option in *LDP*. This option can also be used for solid gears. It is this option that is the focus of comparison here, as it can be considered the most comparable to our models and FE.

In order to calculate the compliances C^i an FE model of each gear is used. The FE model needs to represent the gear geometry in sufficient detail to capture the bending stiffness and base rotation of the teeth. Out of necessity, and given the computing

power at the time, Vedmar (Ref. 12) and Steward (Ref. 7) ran a discrete set of FE models and performed extensive curve fitting on the displacement results in order to calculate equations for the bending compliance for utilization in their tooth contact models. Both used the accurate gear geometry for their FE models; however, both were based on gears using a standard basic rack with no addendum modification. Their methods may be less applicable to non-standard gears. Vedmar considered only a single tooth model and therefore did not include the compliance due to loads on adjacent teeth. Steward included multiple teeth and this compliance was included. Vedmar considered the rim grounded approximately two modules below the root; therefore the gear body deflection was mostly omitted. Steward performed a study of the effect of the gear body compliance with different grounding diameters at the gear bore.

LDP uses an FE model with multiple teeth — but with a tapered straight flank tooth and no fillet radii (Ref. 13). A different FE model is used for each geometry, and so no curve fitting is performed. Compliance with respect to contact points that do not coincide with the finite element mesh are calculated via interpolation using the element shape functions.

In our implementation, the FE mesh for each gear is generated from the exact gear macrogeometry, with no curve fitting of FE results. The FE mesh for the gear is generated using the same code that generates the full FE tooth contact analysis meshes to be discussed later. Via this FE representation, using multiple teeth, the compliance due to loads on adjacent teeth is naturally considered.

One important consideration with the compliance calculated from the FE model is the removal of any "near field" displacements local to the applied loads. When a point load is applied to an FE model node, a local spiked displacement is seen at the node of application. Further, the contact stiffness in these models is represented by an analytical Hertzian model and so these local displacements must be removed from the compliance. Steward and *LDP* (Refs. 7, 13) take the deflection at a corresponding point on the centerline of the tooth, when calculating the FE compliance, via projection of the point normal to the flank in the transverse plane. Vedmar (Ref. 12), in contrast, calculates the compliance with a second FE model where a datum surface a certain distance within the tooth is grounded. The compliance is then calculated by taking the compliance of the original FE model and subtracting the compliance from this model with datum surface grounded. We use this method within our model with the tooth centerline as the datum.

In our model the stiffness with respect to the regular FE grid on the gear flanks is calculated via Guyan reduction of the FE stiffness of the full gear. The stiffness with respect to potential contact points — which will not coincide with the nodes of the regular grid — is interpolated using the shape functions of the FE elements. It is this stiffness with respect to the discretized contact points C^i that is used in Equation 5.

It is only required to perform these steps once for each gear macrogeometry. It is reasonably assumed that the microgeometry modifications do not significantly affect the bending stiffness of the FE model. Therefore microgeometry and misalignments can be changed and the tooth contact analysis re-run without having to recalculate the bending stiffness.

The local contact between potential contact points h_k (F_k) in Equation 5 is considered as a line contact between cylinders. The compression of each tooth between the point of load and the centerline is also included, as this is removed from the stiffness represented by the FE model. In our implementation the approach of Weber (Refs. 15–16) was chosen due to the conclusions of Cornell (Ref. 17) that the Weber method is almost universally used for gear contact and was found to give more consistent results than two other methods investigated by Cornell. Steward (Ref. 7), Vedmar (Ref. 12) and *LDP* (Ref. 13) all use variations of Weber's expression.

If the gears have the same Young's modulus and Poisson's ratio, Weber's expression for the Hertzian deflection normal to the flank at point pair k is given by:

$$h_k(F_k) = \frac{4F_k(1-\nu^2)}{\pi l_k E}\left[\ln\left(\frac{2\sqrt{h_{1k}h_{2k}}}{b_k}\right) - \frac{\nu}{2(1-\nu)}\right] \quad (6)$$

Where:

l_k Length of strip k

ν Poisson ratio

E Young's modulus

h_{ik} Sear length for gear i at strip k; given by the length of a line normal to the gears profile at point k from the centerline of the gear

b_k Half of the Hertzian contact length at strip k

$$b_k(F_k) = \sqrt{\frac{8F_k(1-\nu^2)\,r_{1k}r_{2k}}{\pi l_k E\,(r_{1k}+r_{2k})}} \quad (7)$$

Where:

r_{ik} Radius of curvature on gear i at point k

Figure 3 gives a flow diagram illustrating the main steps in our model.

Loaded Tooth Contact Analysis Model in FE

For validation of our hybrid model, loaded tooth contact analysis was performed in *ANSYS*. Code was written to set up the analysis automatically via a script using the *ANSYS Parametric Design Language* (*APDL*). The geometry was specified in SMT's *MASTA* software (Ref. 18). An algorithm was written to define the FE mesh node locations in the *APDL* script directly from the geometry, avoiding issues which can arise if the geometry is constructed via a CAD model and meshed using automatic meshing tools. Microgeometry flank modifications were included by modifying the node positions before writing them to the script. The algorithm generates a 3-D mesh for a single tooth section first. This mesh is then duplicated, rotated and merged to generate a mesh for multiple teeth. A sufficient number of teeth are included in the FE model to capture the effect of adjacent teeth on those teeth in contact. The rest of the gear blank is generated as a cylinder from bore to root diameter. Misalignment is included by modifying/transforming the node positions.

An algorithm was written to associate the node numbers to element definitions in the script. Solid linear, 8-node hex elements were used for the mesh using *SOLID45* elements. Although *SOLID45* elements are now considered legacy elements, the accuracy of results was checked against models with the now recommended *SOLID185* elements. Further commands

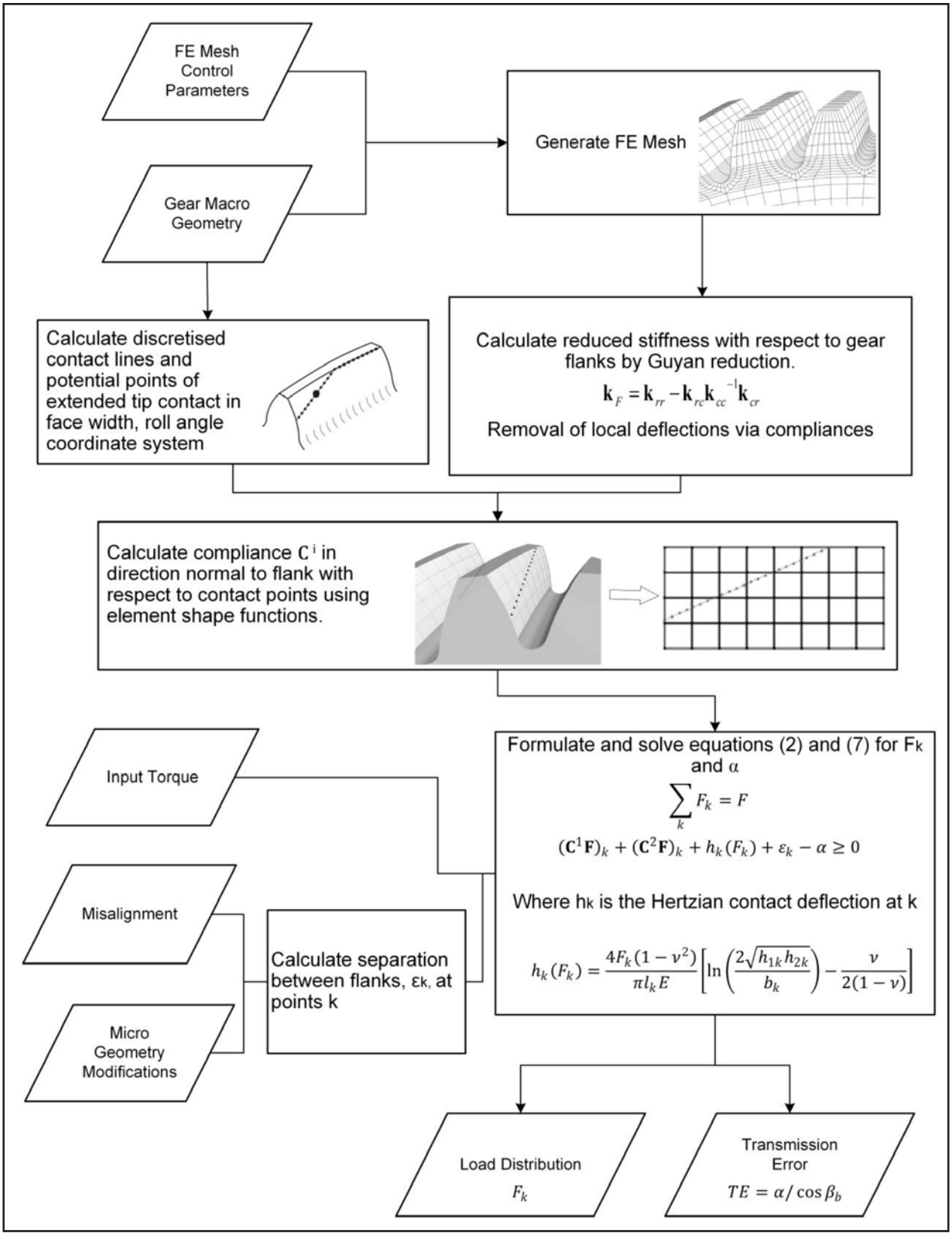

Figure 3 Flow diagram showing main steps in authors gear tooth contact analysis.

were included in the script to translate the wheel and rotate both gears to a meshing position. Backlash was removed by a further rotation of the pinion, as it is not included in the specialized gear tooth contact calculations used.

In order to define the surface to surface contacts between teeth, all nodes on a flank were associated with a named component within the *APDL* script. The potential contacting teeth were calculated given the phase of mesh and the contact ratio. General surface-to-surface contact elements — *TARGE170* and *CONTA173* — were defined between them directly within the script, using the nodal components for these teeth. The Lagrange method was used to maintain the contact constraints purely via Lagrange multipliers; as such, no penetration between contacts was allowed.

Figure 4 shows the boundary conditions applied to the FE model. Zero displacement boundary conditions were applied to all degrees of freedom at the bore of the wheel. The torque was applied at the pinion bore via a pilot node at its center. The pilot node was rigidly connected to the pinion's bore in all degrees of freedom using rigid node-to-surface constraints — *TARGE170* and *CONTA175*. Zero displacement boundary conditions were applied to all degrees of freedom, except rotation about the pinion axis, at the pilot node.

Commands were included within the *APDL* script to rotate

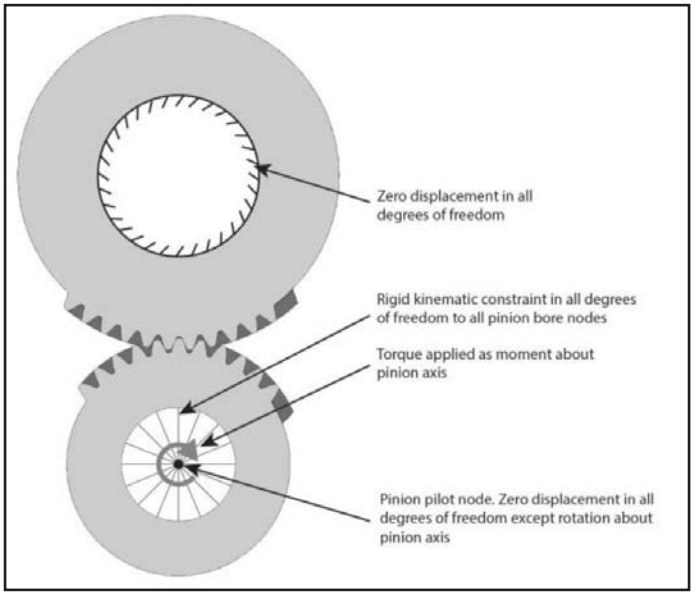

Figure 4 A schematic diagram showing displacement and force boundary conditions applied to FE model.

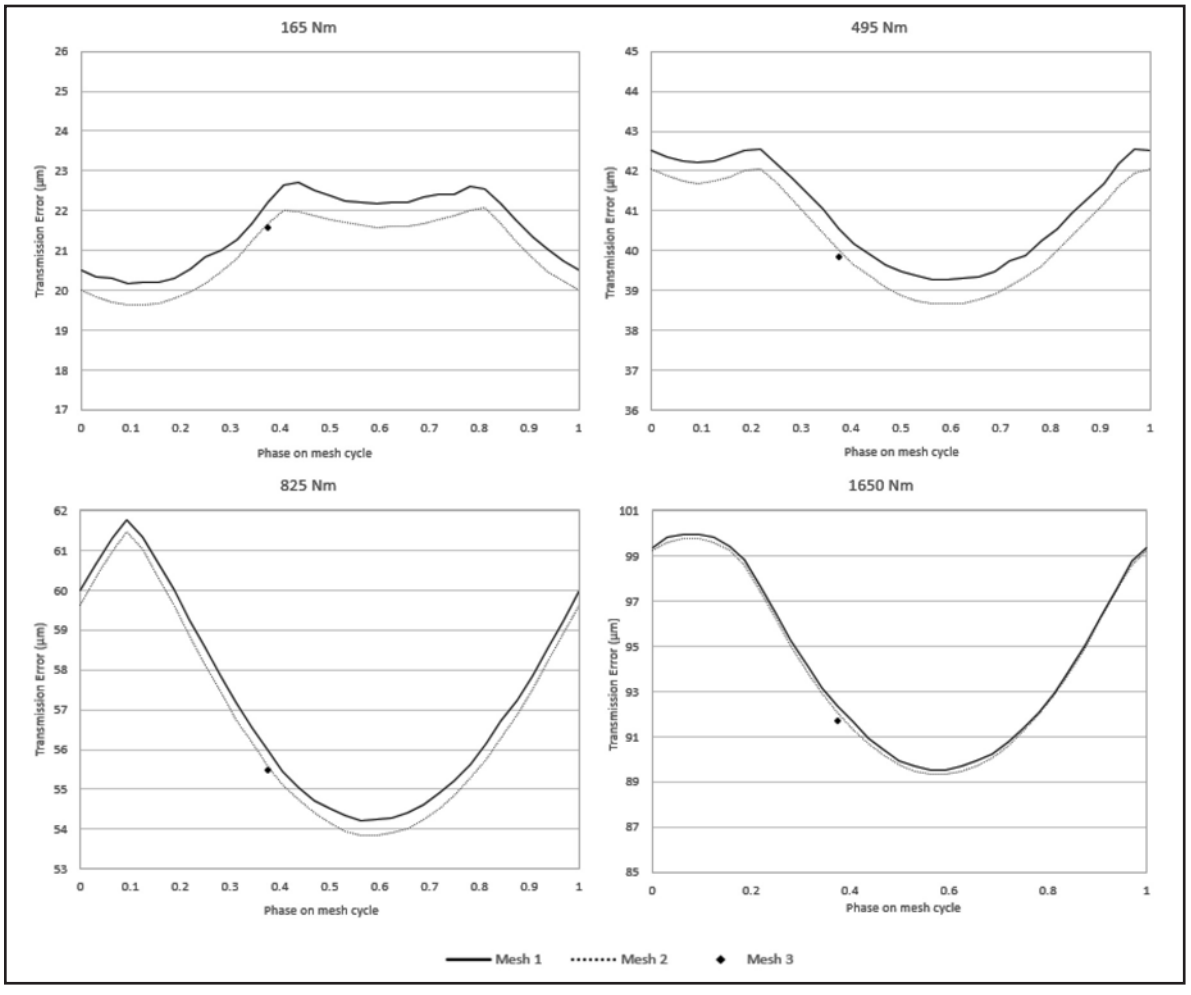

Figure 5 Transmission error results for input torques of 165 Nm; 495 Nm; 825 Nm; and 1650 Nm for Meshes 1, 2 and 3.

the mesh through one base pitch rotation in 32 equal steps. An *ANSYS* model file was saved at each mesh position.

Finally, a static analysis was run at all 32 mesh positions and the rotations of the pinion about its axis were written to file. Linear TE was calculated as the pinion rotation multiplied by its base radius. Geometric non linearity was included in the analysis. Force convergence was checked.

A mesh refinement study was performed for all results. Figure 5 displays results for the transmission error calculated by *ANSYS* for a range of loads for the example introduced later.

The critical area for refinement in a gear tooth contact problem is at the tooth contacts themselves. A mesh fine enough to capture the Hertzian contact deformation is required. For the increasing levels of mesh refinement shown in Figure 5, the mesh was refined in all areas with more refinement at the contacts. Figure 6 shows the contact results for a single phase of the mesh cycle, for the 3 meshes used, at the 1,650 Nm load.

The results in Figure 5 show that the original mesh, Mesh 1, actually captures the deflections and therefore the TE to a sufficient level of accuracy for torques 825 Nm and higher. For lower torques, Mesh 2 results are presented throughout the rest of this study.

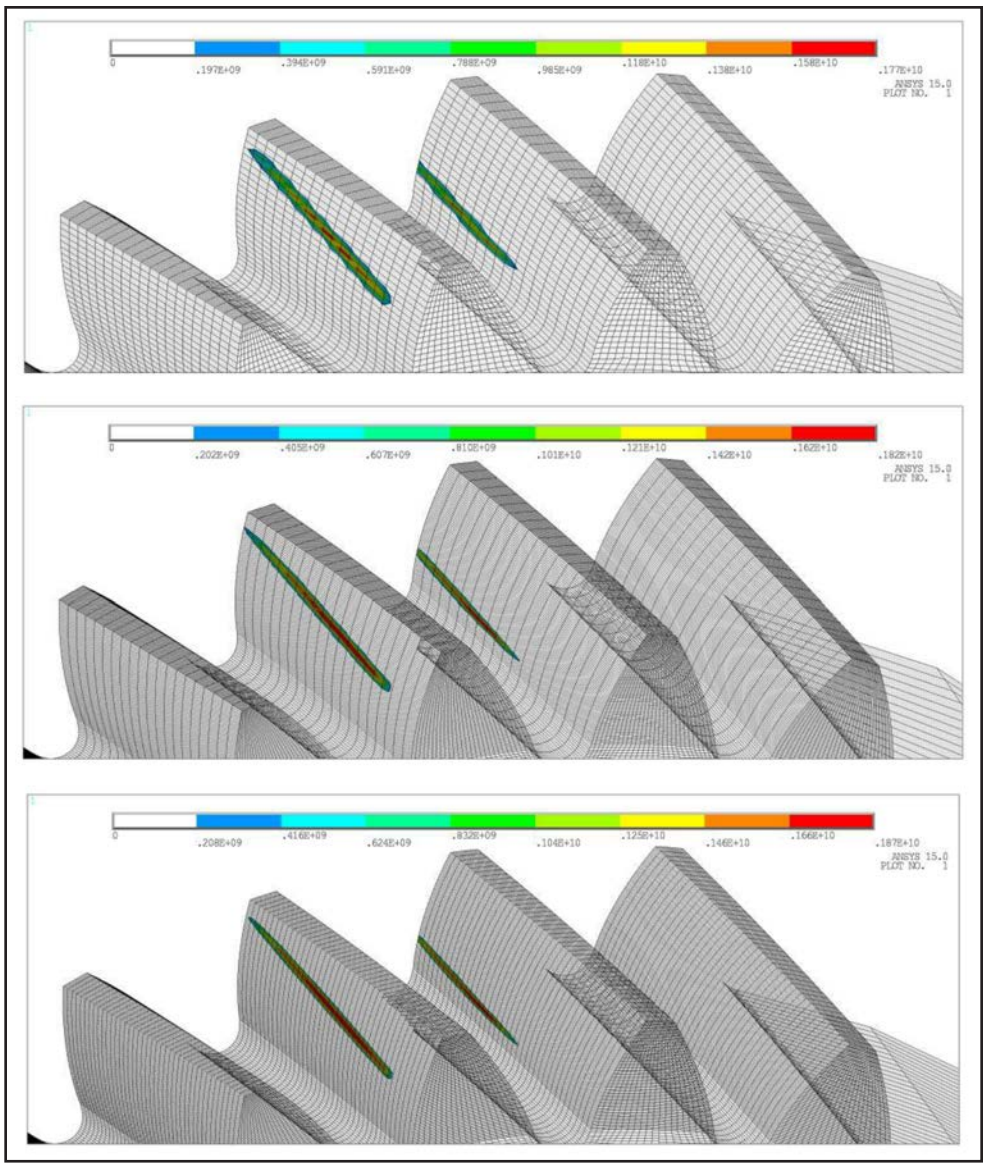

Figure 6 Contact results showing contact stress for 3 meshes considered at single roll angle of 1,650 Nm load case; from top to bottom — Mesh 1, Mesh 2, Mesh 3.

Although dependent on the computing resources available, it is interesting to note the relative run times for the 3 meshes considered. Using a 64-bit system with Intel Xeon Processor E5-2667 @ 2.90 GHz, utilizing 4 of the 6 cores and 128 GB of RAM for 32 mesh positions, the analysis for Mesh 1 ran in approximately 15 hours. Mesh 2 ran in approximately 96 hours, while Mesh 3 took approximately 20 hours to run a single step. This shows why such FE analyses cannot be used as design tools, and why specialized, gear tooth contact models are used extensively in industry.

Results

Helical Gear Pair

Example 1. An example helical gear mesh from a truck application was chosen as our test case. The geometry details for the gear set are given in Table 1.

The microgeometry design, as measured, was considered in all models and analyses. In all analysis models, it was checked

Table 1 Helical gear pair data for example 1.

	Pinion	Wheel
Number of Teeth	29	45
Normal Module (mm)	3.566	
Normal Pressure Angle (degrees)	22.5	
Helix Angle (degrees)	15.778	
Face Width (mm)	30.1	28
Face Width Offset (mm)	2.481	
Centre Distance (mm)	136 501	
Tip Diameter (mm)	116.17	170.97
Root Diameter (mm)	99	154
Cutter Edge Radius (mm)	1.394	0.937
Bore Diameter (mm)	51	78.7
Transverse Tooth Thickness at Reference Diameter (mm)	6.06755	4.86105
Transverse Contact Ratio	1.4915	
Overlap Ratio	0.6195	

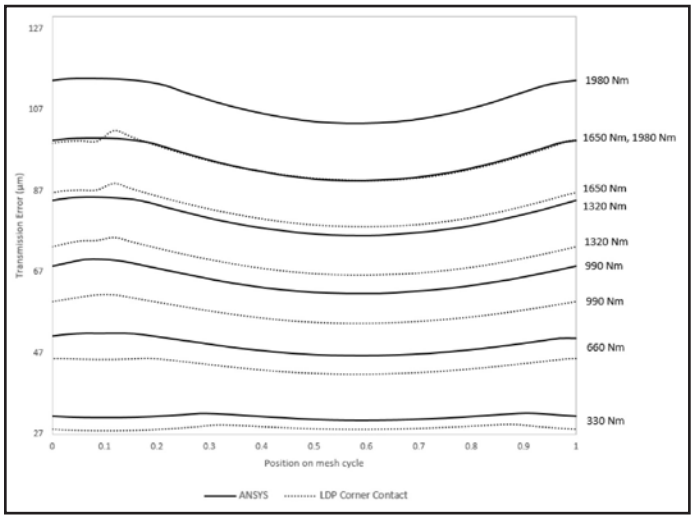

Figure 7 Harris map of calculated transmission errors (TEs) from ANSYS and LDP.

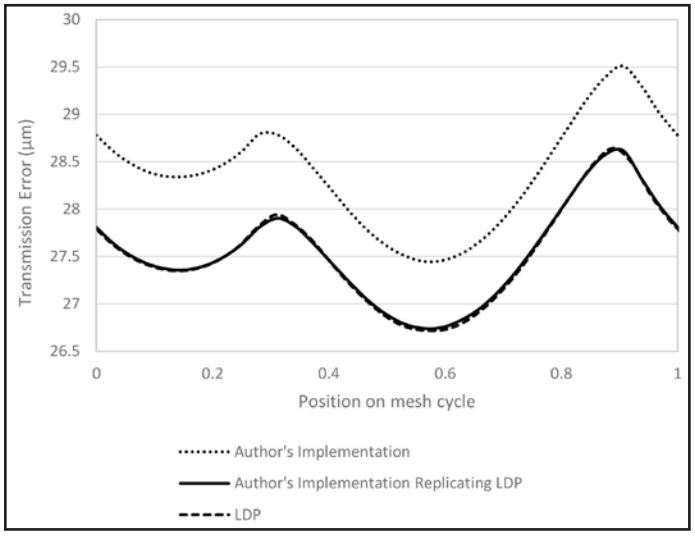

Figure 8 Calculated TE at 1,650 Nm load considering only the Hertzian contact deflection from LDP and the authors' model.

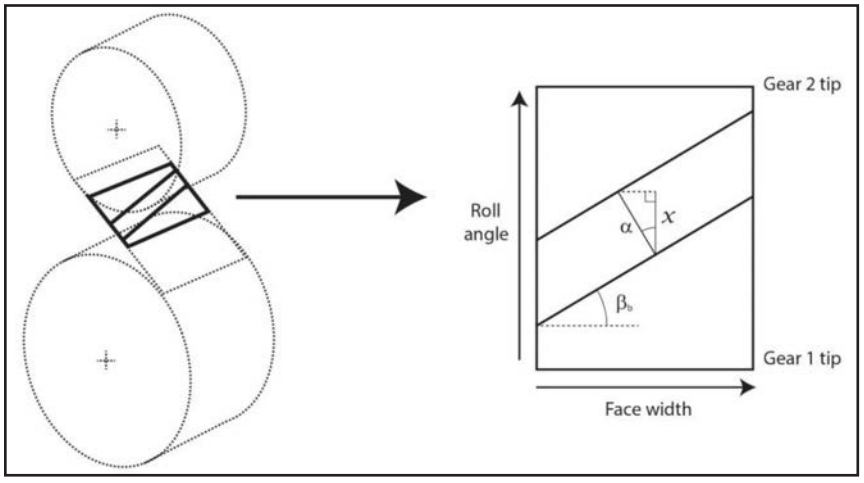

Figure 9 Tangential component of normal rigid body approach shown in the plane of action.

that the relative starting location of the gears was the same. This was done by running the analysis at low load. It was seen that at very low load, as expected given the analysis set up, the minimum transmission error was given by the minimum combined microgeometry modifications within the meshing regions of the flanks, 2.8 µm. This confirmation means that the results of mean transmission errors for all loads should be comparable.

Comparison of LDP and FE. We begin by presenting the FE results as compared to those of a corresponding *LDP* model (*LDP Version 4.6.1* was used for all results within this study). The *LDP* calculations were done using a mesh close to their default values. Unfortunately, a mesh refinement study was not feasible due to limitations of the program. Results from *LDP* are presented with the option for including extended tip contact. Figure 7 presents a Harris map of TE for a range of loads.

It is clear from the results that there is a difference in mean TE between *LDP* and *ANSYS* for all loads, suggesting that *LDP* may be overestimating the mesh stiffness. A possible explanation for this difference is given in the following section.

Comparison of LDP and our hybrid FE and Hertzian models. In order to understand the difference seen in results between *LDP* and FE, we aimed to implement a method that could reproduce the *LDP* results.

To simplify the problem we first considered the calculation ignoring the effect of the bending deflection, i.e. only including deflection due to Hertzian contact. The contact deflections can be isolated in *LDP* by running their tapered plate analysis setting factors for the influence of the tapered plate to 0.

Figure 8 shows the transmission error for the 1650 Nm load case considering the effect of contact deflections only. It is observed from the figure that there is again a significant difference in mean TE between *LDP* and our models. The same behavior was seen at all loads. Figure 8 also shows the results where we do the calculation, as we believe *LDP* is. It is clear that the results are almost identical.

The modifications made in the model "Authors' implementation replicating *LDP*" were made after further investigation of the differences seen. It was identified that a possible explanation lies in the way in which the conversion from normal to transverse plane is done.

In particular, it appears that *LDP* uses the tangential component of the normal rigid body approach as the TE (Fig. 9) i.e.:

$$x = \alpha \cos \beta_b \tag{8}$$

From Figures 2 and 9 this does not appear physically justified and as a result there is a factor of $(\cos \beta_b)^2$ difference between the tangential rigid body approach x (which *LDP* appears to use for the TE) and the TE given by Equation 4.

$$TE = \frac{x}{(\cos \beta_b)^2} \tag{9}$$

Figure 10 shows a comparison of *LDP* with our method replicating *LDP*, including both bending and contact stiffness. Comparison is good. The mean TE is almost identical. A slight difference is seen in the peak-to-peak TE. Peak-

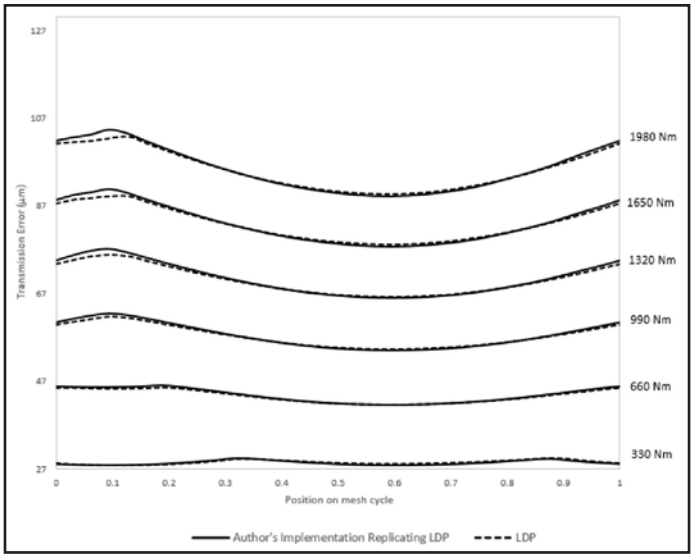

Figure 10 Comparison of calculated TE from LDP and the authors' model replicating LDP.

to-peak TE is very sensitive to the change in stiffness from tip to root. One possible source of this difference is the use of a straight sided tapered tooth in the *LDP* FE model, as compared to the accurate macro geometry used in our implementation.

Given these results, we have potentially identified why the *LDP* results differ from the FE results.

Comparison of hybrid FE and full FE models. In this section we present a comparison between our model, including the relation between TE and rigid body approach according to Equation 4 and FE results. As with the FE results, a mesh refinement study was performed for our models to ensure convergence.

Figure 11 shows a Harris map of the Transmission Error, Figure 12 shows mean TE and Figure 13 the peak-to-peak TE against load.

We see good correlation between our models and the FE analysis. From Figure 13 it is clear that the effect of extended tip contact becomes significant for the peak-to-peak transmission error at loads greater than around 825 Nm. At higher loads, if this effect is not considered, the peak-to-peak transmission error starts to diverge from the FE results and is overestimated.

One possible reason for the slight differences seen between our models and the FE may be the assumption that the contact, except for extended tip contact, lies in the plane of action. In reality gears with profile modifications and deflections under load would contact slightly outside the plane of action (Ref. 19) leading to slightly different gaps being taken up and therefore slightly different transmission errors. Recently, Mahr and Kissling (Ref. 20) suggested applying a correction factor of 0.5 to Weber's formula in such models, this was investigated but no evidence was found in our results to suggest that such a factor should be applied. For our models this factor of 0.5 lead to TE significantly lower than those calculated from FE — especially at the lower loads.

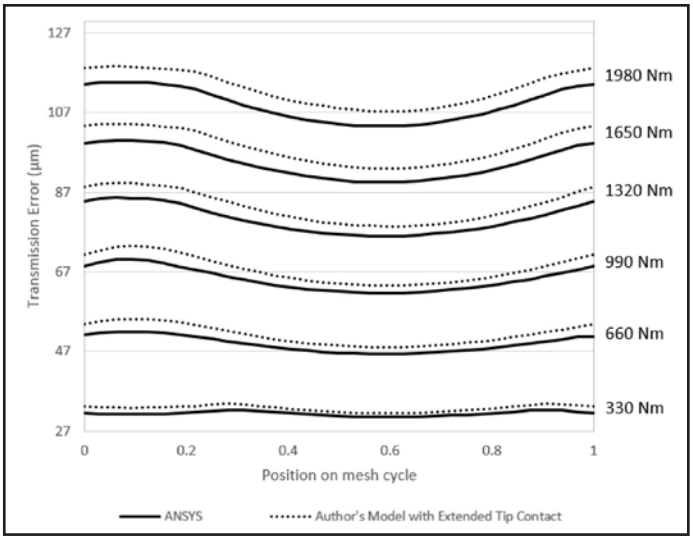

Figure 11 Harris map of calculated TEs from ANSYS and the authors' model with extended tip contact.

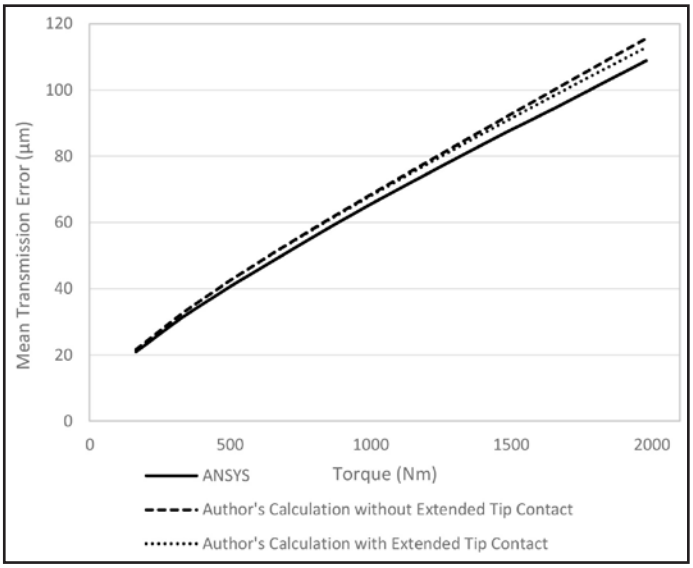

Figure 12 Mean TE from ANSYS and the authors' models against load.

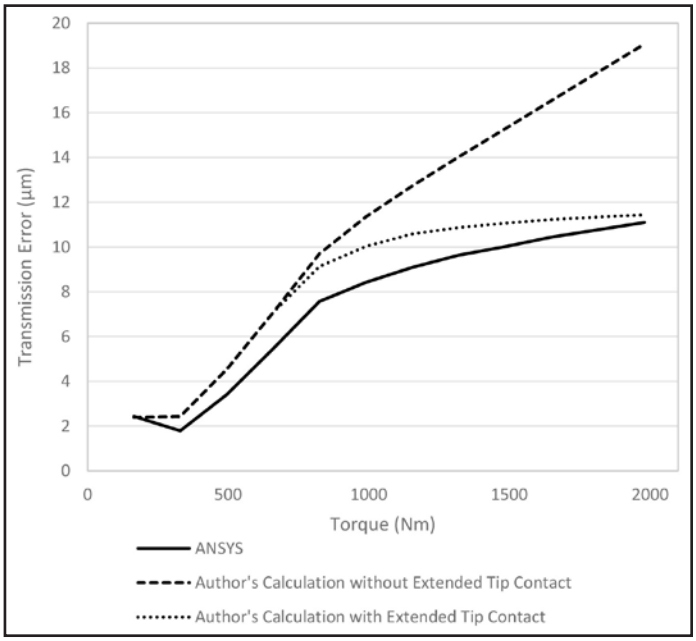

Figure 13 Peak-to-peak TE from ANSYS and the authors' models against load.

Figure 14 shows the calculated contact ratio, against load together with the theoretical contact ratio.

It is seen that for the model including extended tip contact the calculated contact ratio increases under load, due to tooth deflections, and passes the theoretical at around 825 Nm. From Figure 13 we can see that this is the load at which the TE with extended tip contact starts to differ from that without. This is where the additional contact points at the tips of the teeth begin to take significant load. For the model without extended tip contact the calculated contact ratio increases up to the theoretical value but can never exceed it.

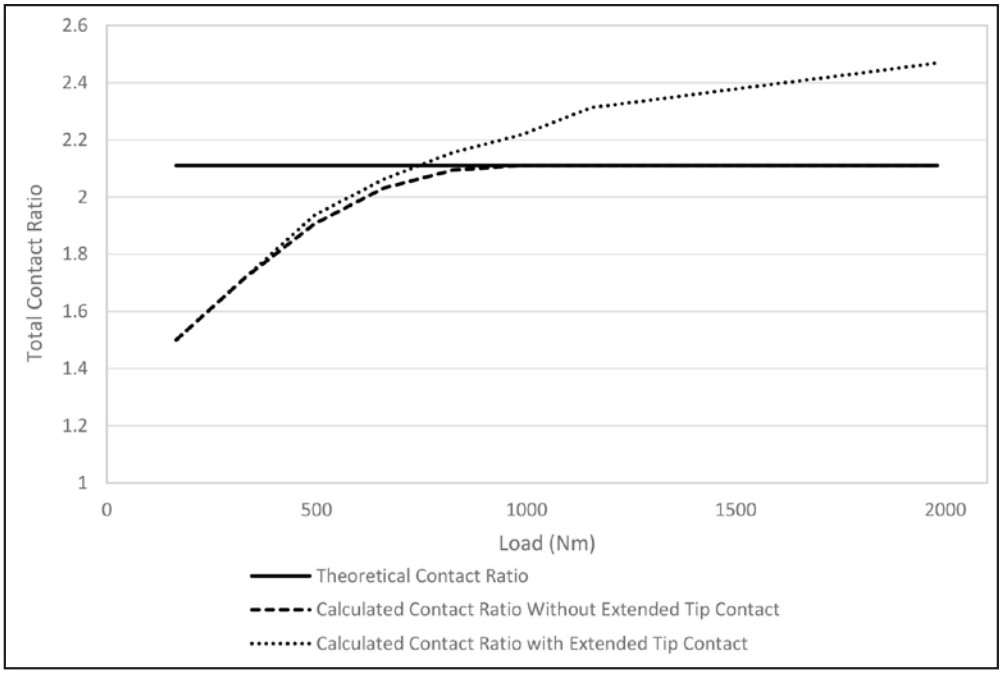

Figure 14 Calculated total contact ratio against load for the authors' models.

Example 2. In this section we consider a second example using some data available in the literature (Ref. 21). Rigaud et al (Ref. 21) develop two hybrid Hertzian and FE-based tooth contact analysis models and compare the results between the two for a gear pair from a truck application. The two models presented include Method 1, using quadratic elements, but only considering coupling between single adjacent teeth, and Method 2, which uses linear elements with curve fitting of displacements and considers the cross-coupling of deflections between all adjacent teeth. We consider comparison of the results shown in Figure 4 (Ref. 21) for the full-bodied example, Model 2, with no misalignment and no microgeometry modifications and under a 1,300 Nm pinion torque.

The details of the gear pair geometry are given in Table 2.

Figure 15 shows a comparison of the transmission error results.

Table 2 Helical gear pair data for example (Ref. 21)

	Pinion	Wheel
Number of Teeth	35	49
Normal Module (mm)	3.5	
Normal Pressure Angle (degrees)	22.5	
Helix Angle (degrees)	21.539	
Face Width (mm)	36.5	
Centre Distance (mm)	158	
Tip Diameter (mm)	138.297	190.897
Root Diameter (mm)	122.247	175.903
Cutter Edge Radius (mm)	0.875	1.225
Bore Diameter (mm)	77	95
Transverse Tooth Thickness at Reference Diameter (mm)	5.911	5.878
Transverse Contact Ratio	1.373	
Overlap Ratio	1.219	

The results confirm the conclusions made in the previous section. The *LDP* results exhibit the same behavior for helical gears as seen in the previous section, i.e. — that the mean TE is lower as compared to the FE results. The authors' model replicating *LDP* agrees well with the *LDP* results.

The Rigaud results appear to be closer to those of *LDP* than to those of *ANSYS*. Further, the difference between *LDP* and Rigaud results appears to be within the range of mesh refinement. We have similarly reproduced close to the results of Rigaud with a change of mesh. This suggests that Rigaud may have used the same conversion of deflections in the normal plane to those in the

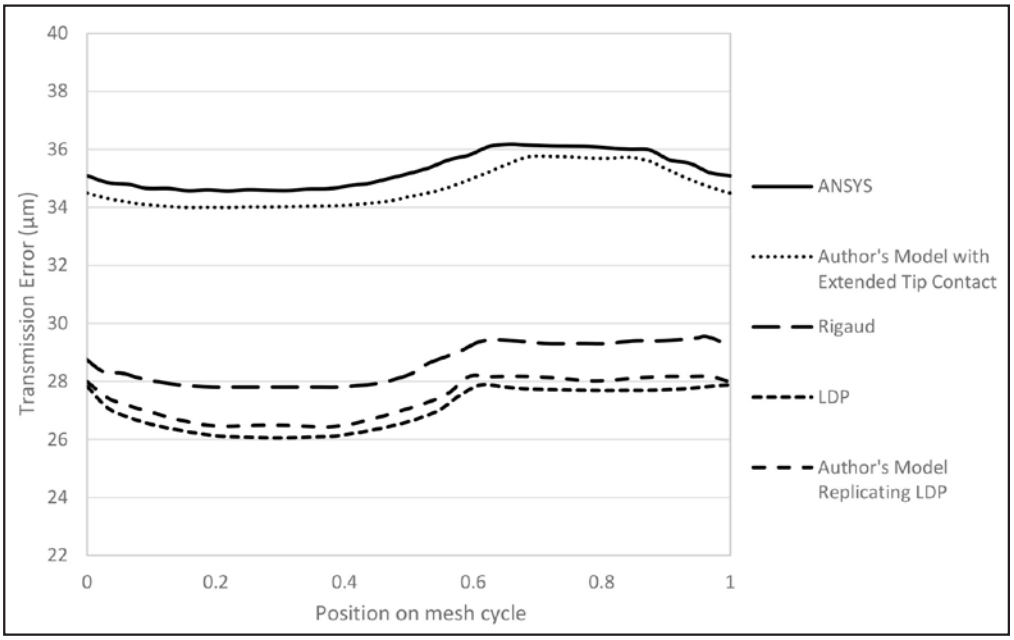

Figure 15 Comparison of TE between ANSYS, LDP, Rigaud and the authors' models for the 1,300 Nm load.

transverse plane as *LDP*.

The *ANSYS* results match our hybrid implementation including the effect of extended tip contact closely.

Conclusion

- A specialized gear tooth contact analysis model based on hybrid FE and Hertzian contact formalism has been presented, with particular focus on helical gears.
- An extensive comparison was presented between the results of this model and a 3-D FE tooth contact analysis using *ANSYS* showing good correlation in TE. These results reinforce the use of such models as efficient design tools that can be run in time scales orders of magnitude quicker than FE tooth contact analyses, while retaining similar accuracy. The presented solution has been implemented in SMT's *MASTA (MASTA Version 7.0* was used for the results in this study*)* software (Ref. 18).
- It was shown that, particularly for the case of low helix angle helical gears under consideration, the extended off line of action tooth contact at the gear tips plays a critical role in the transmission error at higher loads.
- Further comparison has also been made with the results of the well-known tooth contact analysis program, *LDP*. It was observed that *LDP* appears to underestimate the mean transmission error as compared to the FE. A possible explanation for this difference, as a difference in the conversion from normal to transverse plane, was proposed. It was shown, via modifications to the authors' models, that this proposed difference could lead to the results observed.

References

1. Welbourn, D.B. "Fundamental Knowledge of Gear Noise: A Survey" (No. IMechE-C117/79), 1979.
2. Houser, D.R. "Gear Noise Sources and Their Prediction Using Mathematical Models," Gear Dynamics and Gear Noise Research Laboratory, Ohio State Univ., 1985.
3. Houser, D.R. "Gear Noise — State of the Art," *INTERNOISE and NOISE-CON Congress and Conference Proceedings* (Vol. 1988, No. 4, pp. 601-606), Institute of Noise Control Engineering, 1988.
4. Houser, D.R. *User's Guide* for The OSU *Load Distribution Program* (*LDP*), *Shaft Analysis Program*, and *RMC*, 2011.
5. Conry, T.F. and A. Seireg. "A Mathematical Programming Method for Design of Elastic Bodies in Contact," *Journal of Applied Mechanics*, 38(2), pp.387-392, 1971, *http://dx.doi.org/10.1115/1.3408787*.
6. Seager, D.L. "Separation of Gear Teeth in Approach and Recess; Likelihood of Corner Contact," *ASLE Transactions*, 19(2), pp.164-170, 1976, *http://dx.doi.org/10.1080/05698197608982790*.
7. Steward, J.H. "Elastic Analysis of Load Distribution in Wide-Faced Spur Gears," 1989.
8. Steward, J.H. "The Compliance of Solid, Wide-Faced Spur Gears," *ASME J. Mech. Des*, 112, pp.590-595, 1990, *http://dx.doi.org/10.1115/1.2912651*.
9. Lin, H.H, J. Wang, F.B. Oswald and J.J. Coy. "Effect of Extended Tooth Contact on the Modeling of Spur Gear Transmissions," 1993, National Aeronautics and Space Administration.
10. Singh, A. and D.R. Houser. "Analysis of Off-Line-Of-Action Contact at the Tips of Gear Teeth" (No. 941761), SAE Technical Paper, 1994, *http://dx.doi.org/10.4271/941761*.
11. Munro, R.G., L. Morrish and D. Palmer. "Gear Transmission Error Outside the Normal Path of Contact Due to Corner and Top Contact," *Proceedings of the Institution of Mechanical Engineers*, Part C: *Journal of Mechanical Engineering Science*, 213 (4), pp.389-400, 1999, *http://dx.doi.org/10.1243/0954406991522347*.
12. Vedmar, L. "On the Design of External Involute Helical Gears," 1981, NA.
13. Prabhu, M.S. "Load Distribution and Transmission Error in Thin-Rimmed Gears through Finite Element Analysis," 1994.
14. Prabhu, M.S. and D.D.R. Houser. "A Hybrid Finite Element Approach for Analyzing the Load Distribution and Transmission Error in Thin-Rimmed Gears," *VDI BERICHTE*, 1230, 1996, pp.201-212.
15. Weber, C., 1949. "The Deformation of Loaded Gears and the Effect of Their Load Carrying Capacity," Sponsored Research (Germany), British Dept. of Scientific and Industrial Research, Report No. 3, 1949.
16. Weber, C. and K. Banaschek. "The Deformation of Loaded Gears and the Effect of Their Load Carrying Capacity," Department of Scientific and Industrial Research, 1951.
17. Cornell, R.W. "Compliance and Stress Sensitivity of Spur Gear Teeth," *Journal of Mechanical Design*, 103 (2), pp.447-459, 1981, *http://dx.doi.org/10.1115/1.3254939*.
18. *www.smartmt.com/masta*.
19. Wink, C.H. and A.L. Serpa. "Investigation of Tooth Contact Deviations from the Plane of Action and Their Effects on Gear Transmission Error," *Proceedings of the Institution of Mechanical Engineers*, Part C: *Journal of Mechanical Engineering Science*, 219 (5), pp.501-509, 2005, *http://dx.doi.org/10.1243/095440605X16983*.
20. Mahr, B. and U. Kissling. "Comparison between Different Commercial Gear Tooth Contact Analysis Software Packages," unpublished manuscript.
21. Rigaud, E. and D. Barday. "Modeling and Analysis of Static Transmission Error; Effect of Wheel Body Deformation and Interactions between Adjacent Loaded Teeth," *4th World Congress on Gearing and Power Transmission*, Paris, 1999 (Vol. 3, pp. 1961-1972).

For Related Articles Search

tooth contact analysis

at **www.geartechnology.com**

Dr. Paul Langlois is the CAE products development department manager at SMT. Having worked for SMT for 10 years, he has extensive knowledge of transmission analysis methods and their software implementation. He manages the development of SMT's software products and is a main contributor to many aspects of the technical software development. As a member of the BSI MCE/005 committee, Langlois contributes to ISO standards development for gears.

Baydu Al has worked since October 2014 as an analyst/software engineer at Smart Manufacturing Technology Ltd. (SMT). He previously worked as a researcher at Nottingham University in gas turbine and transmission systems, specializing in efficiency and oil management. Upon joining SMT, Al has been contributing to MASTA's loaded tooth contact analysis as well as the analysis of tooth interior fatigue fracture.

Dr. Owen Harris, a graduate of Trinity College Cambridge, has worked in the analysis of transmissions and geared systems for over fifteen years. He was instrumental in writing some of the first commercial software codes for housing influence, system modal analysis and gear whine and planetary load sharing. Harris has filled many roles in over ten years working at Smart Manufacturing Technology Ltd. (SMT). He has worked on SMT's state-of-the-art MASTA software, while at the same time being heavily involved in many engineering projects. Harris's current focus is to lead SMT's research department.